Nuclear spin relaxation in a vinylidene fluoride and trifluoroethylene copolymer 70/30 - I. Dynamics and morphology in the ferroelectric phase

Jérôme Hirschinger, Bernard Meurer, Gilbert Weill

Classification
Physics Abstracts
61.40 — 76.60 — 77.80B

Nuclear spin relaxation in a vinylidene fluoride and trifluoroethylene copolymer 70/30 I. Dynamics and morphology in the ferroelectric phase

Jérôme Hirschinger, Bernard Meurer and Gilbert Weill

Institut Charles-Sadron (CRM-EAHP), CNRS-ULP Strasbourg, 6, rue Boussingault, 67083 Strasbourg Cedex, France

(*Reçu le 19 avril 1988, accepté sous forme définitive le 7 octobre 1988*)

Résumé. — La dynamique des spins nucléaires du proton et du fluor dans un copolymère de fluorure de polyvinylidène et de trifluoroéthylène 70/30 a été caractérisée par une série de mesures de formes des précessions libres, de temps de relaxation spin réseau T_1 dans le référentiel du laboratoire et $T_{1\rho}^{\theta}$ dans des référentiels tournants, des mesures d'effet Overhauser transitoire. La variation de $T_{1\rho}^{\theta}$ en fonction de θ met en évidence l'existence de mouvements locaux au sein des crystallites impliquant l'existence de « défauts » cristallins. Un modèle simple, traitant de manière analogue les effets de relaxation croisée et de diffusion de spin permet d'analyser quantitativement l'ensemble des données. Cette analyse montre les mêmes mouvements de haute fréquence dans la phase amorphe en dessous du point de Curie et dans l'ensemble de la phase paraélectrique (au-dessus du point de Curie).

Abstract. — The spin dynamics of hydrogen and fluorine in a 70/30 VF_2/TrFE copolymer have been investigated by the measurements of the nuclear spin-lattice relaxation times in the laboratory (T_1) and rotating frames ($T_{1\rho}^{\theta}$) the transient Overhauser effect (TOE) and the free induction decay (FID). $T_{1\rho}^{\theta}$ results demonstrate the presence of local motions within the crystallites implying the existence of crystalline « defects ». A simple model treating cross-relaxation and spin diffusion on an equal footing was found to be appropriate to describe all the relaxation data in the laboratory frame. Moreover, it confirms that the high frequency motions in the amorphous phase below the Curie point and in the paraelectric phase are of the same type.

1. Introduction.

Polyvinylidene fluoride (PVF_2) is known to possess a polar crystalline β phase were the chains are in the all-trans conformation packed with no symmetry center in the unit cell [1]. The ferroelectricity and piezoelectricity of this system have been extensively studied [1]. Recently, it has been shown that vinylidene fluoride trifluoroethylene copolymers P(VF_2-TrFE) have the same properties but undergo a ferroelectric — to — paraelectric phase transition well below the melting point T_m [2]. This paper is devoted to the study of the molecular dynamics by nuclear magnetic resonance in a VF_2/TrFE copolymer (70/30 mol %) below the Curie

point T_c. The NMR study of the paraelectric phase is presented in reference [3] hereafter referred to as Part. II.

The general relation between the relaxation times of the nuclear magnetization and the spectral density $J(\omega)$ of the molecular motions contributing to the fluctuations of the local dipolar field H_L is well known [4]. Its application to polymers containing both hydrogen and fluorine nuclei is however difficult due to :

(i) the existence of, at least, two phases (crystalline and amorphous) where the molecular motions may be different ;

(ii) the fact that spin-lattice relaxation in the two phases is coupled by spin diffusion so that one cannot, in principle, consider a nonexponential decay as the sum of the independent relaxations in each phase [5] ;

(iii) and, finally, the presence of two spin species with large gyromagnetic ratios γ (^{1}H and ^{19}F) interacting by cross-relaxation which can be alone responsible for a nonexponential relaxation [6].

Precious information is then provided by the measurements of the free induction decay (FID) and the spin-lattice relaxation in the rotating frame ($T_{1\rho}$), neither of which show the nonexponential cross-relaxation effects. Moreover, the spin diffusion rate can be varied in the $T_{1\rho}^{\theta}$ experiments [7, 8] (see Sect. 4.1). In order to account simultaneously for cross-relaxation and spin diffusion effects on relaxation in the laboratory frame we use a phenomenological model based on a similar form for the coupling between magnetizations of the two phases and magnetizations of the two spins species. By numerical analysis, this model is compared to the experimental data resulting from both the inversion recovery sequence (IR) applied to the ^{1}H or ^{19}F spin system and the transient Overhauser effect (TOE).

2. Experimental.

2.1 SAMPLES. — The P(VF_2-TrFE) 70/30 copolymer, with mean molecular weight $M_n = 55\,000$ and $M_w/M_n = 1.9$, has been provided by Atochem Co. (France). Unoriented thick films (1 600 μm) of copolymer have been cast at 180 °C in Thomson CSF Laboratories and quenched at room temperature. Subsequent rolling produced oriented films of 470 μm thickness with biaxial orientation of the crystal axes. The unoriented and oriented samples were then annealed at 130 °C. Wide-angle X-ray diffraction reveals that the orientation becomes uniaxial [9] (draw ratio $\simeq$ 3.5/1) i.e. the sample exhibits cylindrical symmetry about the draw axis.

2.2 SPECTROMETER AND DATA ANALYSIS. — NMR measurements have been carried out on a Bruker SXP spectrometer with a V3601-1 Varian electromagnet operating from 4 to 60 MHz. The resonance field H_0 is controlled within 0.5 μT by a field frequency lock (Drush, RMN gaussmeter and regulation unit TA02) allowing phase detection with quadrature receivers at all operating frequencies. The FID signal is digitized with a converter Bruker BC 100 q fitted with two consecutive sampling rate (8 bits ; up to 10 MHz sampling frequencies). The data are averaged and treated on-line on a Nicolet BNC 12 minicomputer. For the transient Overhauser experiments [6], and additional system has been built : it is composed of a Hewlett Packard signal generator followed by Anzac modulators (Two double balanced mixers give an isolation of 60 dB), a Kalmus amplifier (30 dB gain) and a Power Lab RF power amplifier (22 dB gain). The net output is 500 W in class A(CW).

In order to control the pulse duration we also used a second preamplifier and receiver allowing a simultaneous recording of the ^{1}H and ^{19}F signals. The corresponding probe includes two crossed coils cemented on the two walls of the glass supporting tube, a solenoïd of 8 mm

diameter tuned to hydrogen resonance (60 MHz) and a saddle coil of 12 mm diameter tuned to fluorine resonance (56.4 MHz) with a home-built tubular capacitor (11 ± 2 pF). This probe withstands 2 and 4 μs $\pi/2$ pulse duration, in, respectively, ^{1}H and ^{19}F resonance.

The cross-relaxation between ^{1}H and ^{19}F spin systems has been measured according to Solomon [6] by the application of a π pulse at time $\tau = 0$ at the resonant frequency of the fluorine spins followed by a $\pi/2$ pulse applied on the hydrogen nuclei at time τ. The IR $\pi - \tau - \pi/2$ pulse sequence was used to measure T_1 with a series of home-built probes operating from 6 to 60 MHz. For the $T_{1\rho}^{\theta}$ experiment [8, 10], the ^{1}H spins were spin-locked by applying a pulse of length τp followed by a 90° phase shifted pulse of duration τ off resonance. τp is adjusted to maximize the spin-locked magnetization. Both the magnitude of the radiofrequency field H_1 measured by the length of a π pulse and the off resonance frequency define the effective spin-lock field H_e and the spin-lock angle θ (see Sect. 4.1). $T_{1\rho}^{\theta}$ is then measured by observing the decay of the magnetization component perpendicular to H_0 as a function of the spin-lock duration τ.

The treatment of the FID signal is described in references [11] and [12]. The spin-lattice relaxation decays are fitted by non-linear least-squares adjustments of 3 to 5 parameters to a sum of exponentials, $A \cdot \exp(-B\tau) + C \cdot \exp(-D\tau) + E$. The sampling of the exponentials is optimized by changing the increment of the evolution periods τ as necessary (Fig. 1).

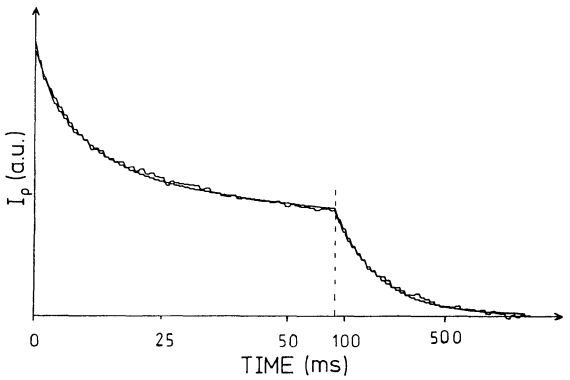

Fig. 1. — ^{1}H relaxation in the rotating frame by the spin-lock sequence with $H_e = 12$ G and $\theta = 50°$ at 27 °C ($\nu_L = 60$ MHz). The two exponentials require two time scales for a better sampling and data analysis (here, 1 ms and 20 ms increments). Fitted parameters : $T_{1\rho S} = (8.5 \pm 0.5)$ ms, $T_{1\rho L} = (198 \pm 8)$ ms and $I_{L\rho} = (54 \pm 2)$ %.

3. Results.

3.1 $T_{1\rho}$ RELAXATION DATA. — The relaxation decays fit well to two exponential curves (Fig. 1). A minimum is observed in the short and long ^{1}H $T_{1\rho}$ components at, respectively, 5 and − 10 °C for $H_1 = 12$ G (Fig. 4). The long component $I_{L\rho}$ which is about 55 % below 70 °C, goes up, reaches 75 % near the 100 °C, drops suddenly and totally disappears at 115 °C (Fig. 8). We have checked that the same intensity ($I_L \simeq 55$ %) is obtained at room temperature with $H_1 = 24$ G and in ^{19}F resonance. Figure 5 shows that variation of the two ^{1}H $T_{1\rho}$ components as a function of the spin-lock angle θ is different. While the short

component $(T_{1\rho}^{\theta})_S$ increases steadily with decreasing θ, there is a clear maximum of the long component $(T_{1\rho}^{\theta})_L$ around 50°. The long component intensity $I_{L\rho}$ is found to be independent of θ (Fig. 6).

3.2 T_1 RELAXATION DATA. — When the ^1H Larmor frequency $\nu_L = \omega/2\pi$ is equal to 8, 21 and 60 MHz two exponential components can be separated (Fig. 2) above − 30, and 7 °C, respectively. While the long component T_{1L} decreases with increasing temperature until the phase transition is reached, for these three frequencies, the short component T_{1S} shows a minimum at 17, 35 and 60 °C (Fig. 7). T_{1L} and T_{1S} are longer in ^{19}F resonance (56.4 MHz) but their temperature variations remain similar. Figure 8 shows that it is the short component which appears at about − 30 °C. This is particularly evident on the data at 21 MHz. At 60 MHz, a separation into two components is outside experimental accuracy at low temperatures since the two relaxation times become too close to each other. It is nevertheless obvious that I_L decreases when ν_L decreases from 60 to 21 MHz. At 8 MHz, I_L (≃ 45 %) is surely an underestimate since, due to the considerable deadtime, only the relaxation of the tail of the FID is observable (see Sect. 4).

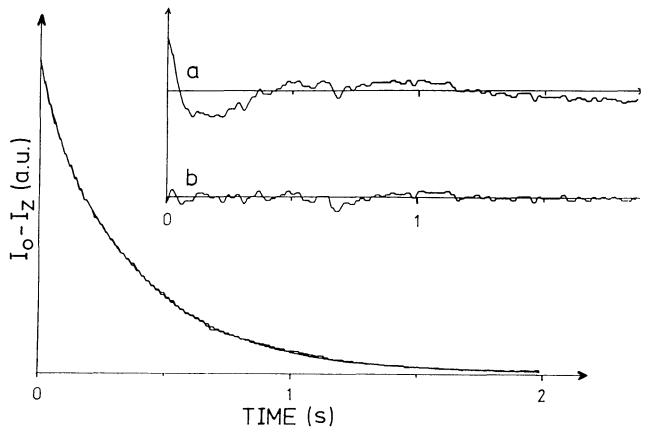

Fig. 2. — ^1H relaxation in the laboratory frame by the IR sequence with ν_L = 60 MHz at 27 °C. The distribution of the residuals for a one (a) and two (b) — exponential fit in the insert clearly demonstrates the two-exponential nature of the decay. Fitted parameters : T_{1S} = (80 ± 2) ms, T_{1L} = (390 ± 40) ms and I_L = (80 ± 3) %.

3.3 CROSS-RELAXATION DATA. — The transient Overhauser decays have been successfully fitted to Solomon's equations [6, 13, 14] with the difference of two exponentials

$$I_+ \{\exp(-\tau/T_{1+}) - \exp(-\tau/T_{1-})\}$$

with $T_{1+} < T_{1-}$ (four-parameter fit). T_{1+}, T_{1-} and I_+ are decreasing as the temperature rises from − 100 to 70 °C. The determination of these quantities is not possible above 70 °C because of the weakness of the cross-relaxation effect ($I_+ \simeq 0$) (Figs. 9 and 10).

4. Interpretation of the results.

4.1 RELAXATION IN THE ROTATING FRAME. — For a spin-lock sequence at an angle θ in the weak collision limit i.e. as long as H_e^2 is much higher than H_L^2 or the correlation time of the

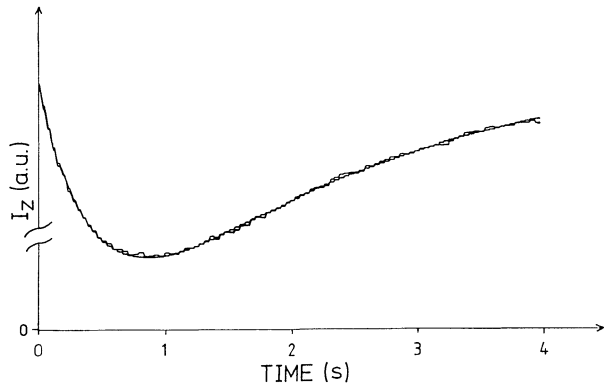

Fig. 3. — ^{1}H relaxation in the laboratory frame by the TOE sequence with $\nu_L = 60$ MHz at − 11 °C. The two-exponential fitting to the data with four parameters gives $T_{1+} = (0.45 \pm 0.02)$ s, $T_{1-} = (2.0 \pm 0.1)$ s and $I_+ = (64 \pm 2)$ %.

molecular motion τ_c is much smaller than the rigid-lattice transverse relaxation time $T_{2\,RL}$; and if we assume as usual that the motion of all the internuclear vectors in one phase are described by the same autocorrelation function $\theta(\tau)$ it is found [10] from the ^{1}H resonance ($\omega \gg \omega_e$)

$$(T_{1\rho}^{\theta})^{-1} = \{\Delta M_2^{HH} \sin^2\theta \cos^2\theta + \Delta M_2^{HF} \sin^2\theta\}\, J(\omega_e) + \Delta M_2^{HH} \sin^4\theta J(2\omega_e) + f(\omega, \theta) \tag{1}$$

where $J(\omega)$ is the Fourier transform of $\theta(\tau)$; $\omega_e = \gamma H_e$ with $H_e^2 = H_1^2 + h^2$, h is the off-resonance field (when $\theta = 90°$, $H_e = H_1$ and $T_{1\rho}^{\theta} = T_{1\rho}$) ; $f(\omega, \theta)$ is the sum of spectral density terms around ω which can be approximated by ρ (Eq. (5)) provided that $J(\omega_e) \gg J(\omega)$ i.e. $\rho \ll (T_{1\rho})^{-1}$ (when $\theta = 0°$, $(T_{1\rho})^{-1} = f(\omega, \theta) = \rho$). ΔM_2^{HH}, ΔM_2^{FF} and ΔM_2^{HF} are ; respectively, the ^{1}H, ^{19}F homonuclear and ^{1}H heteronuclear second moment fractions that are modulated by the molecular motion.

The two-exponential $T_{1\rho}^{\theta}$ relaxation can only be due to the composite nature of our polymeric system since no cross relaxation nonexponential effects operate in the rotating frame [10, 15]. The analysis of the FID signals after different spin-lock durations clearly shows that the long and short components are respectively associated with the crystalline and amorphous phases [11]. H_e^2 is much higher than H_L^2 so that the intrinsic relaxation times in each phases should be given by equation (1). Since the T_1 components at 60 MHz (Fig. 7) are much longer than the $T_{1\rho}$ components (Fig. 4), $f(\omega, \theta)$ can be replaced by ρ.

Furthermore, one notes that the more important increase of $T_{1\rho}$ with decreasing θ at high angles ($\theta > 50°$) is obtained when $J(\omega_e) = J(2\omega_e)$. It is noted that this condition is, at least approximately, fulfilled when $\omega_e \tau_c \ll 1$. In this case, we can rewrite equation (1)

$$(T_{1\rho})^{-1} = C \sin^2\theta + \rho \tag{2}$$

where C is constant.

Figure 5b shows effectively that such a variation is consistent with the $(T_{1\rho}^{\theta})_S$ data. On the other hand, equation (2) is unable to fit the $(T_{1\rho}^{\theta})_L$ results (Fig. 5a) : the experimental values for $\theta > 50°$ are higher than the highest expected data. In addition, the obvious maximum of $(T_{1\rho}^{\theta})_L$ near the « magic angle » $\theta_m = 54.7°$ cannot be accounted for by equation (1). This

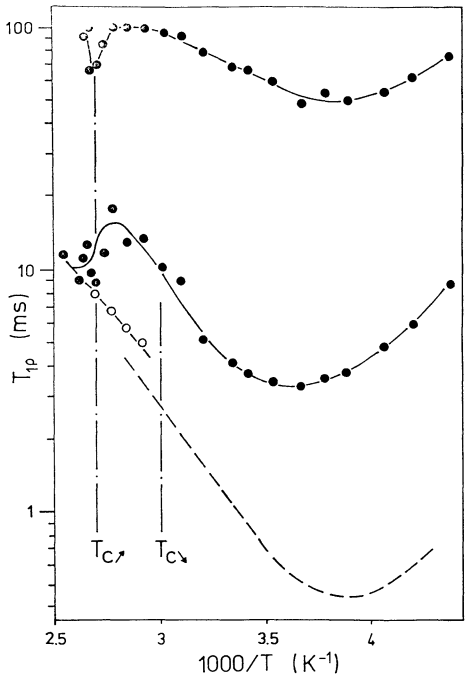

Fig. 4. — ^{1}H $T_{1\rho}$ data as a function of temperature ($\theta = 90°$, $\nu_L = 60$ MHz, $H_1 = 12$ G). The broken curve shows the calculated $T_{1\rho S}$ variation for the HP correlation function according to the relaxation in the laboratory frame (Sect. 4.2.3).

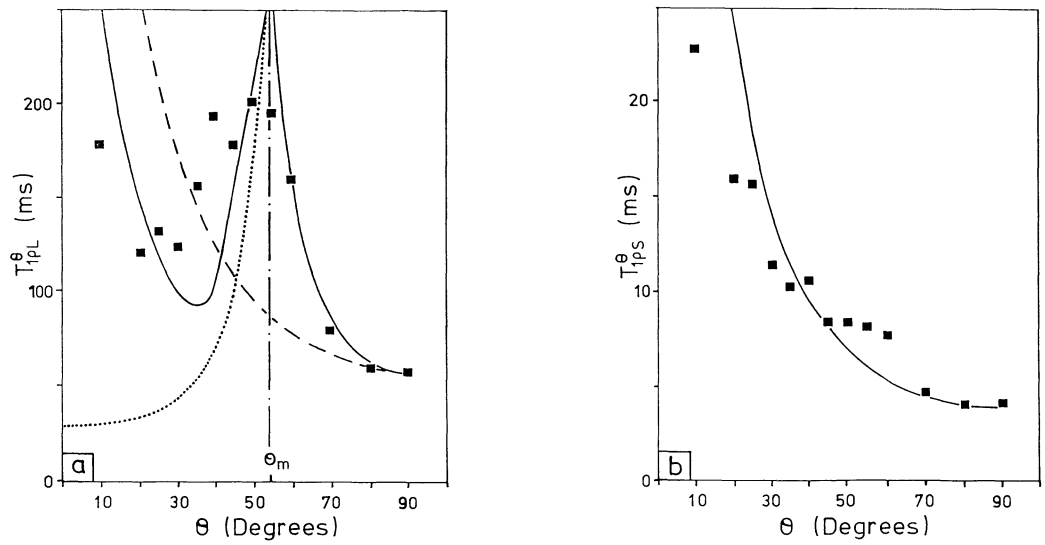

Fig. 5. — ^{1}H $T^{\theta}_{1\rho}$ data as a function of the spin-lock angle θ at 27 °C with a constant $H_e = 12$ G at 60 MHz. (a) Broken curve : the relaxation step only (Eq. (2), $C = 15\ s^{-1}$) ; dotted curve (when deviating from the full curve) : the spin diffusion step only (Eq. (3), $K' = 17\ s^{-1}$) ; full curve : the two following steps ($C = 50\ s^{-1}$ and $K' = 25\ s^{-1}$). (b) The full curve represents the computed variation according to equation (2), $C = 250\ s^{-1}$).

characteristic behavior is believed to be reminiscent of the spin diffusion effect. Indeed, since $H_e^2 \gg H_L^2$ the spin diffusion rate R is controlled by the secular part of the spin-spin interaction which vanishes for $\theta = \theta_m^{16}$ and

$$R = K(3\cos^2\theta - 1) \tag{3}$$

where K is a constant.

We shall then assume that the relaxation in the crystalline phase occurs *via* spin diffusion towards « sinks ». A sink is a part of the material where the relaxation is very fast i.e. where there is molecular motion. Since $(T_{1\rho}^{\theta})_S$ is quite short, the amorphous regions could be efficient sinks. In this case, $(T_{1\rho}^{\theta})^{-1}$ is equal to the spin diffusion rate R [5]. It is seen in figure 5a, that, although the maximum of $(T_{1\rho}^{\theta})_L$ at θ_m is then well described, the predicted values are much too weak at small angles. This implies that diffusion towards the sinks is not the rate-controlling step. Since relaxation times are expected to decrease with decreasing θ (Eq. (1) and (2)) the loss in the effectiveness of the sink is not likely to be the results of intrinsic crystalline relaxation.

An explanation could be that the amorphous regions should not be considered as efficient sinks when θ becomes less than 30°. However, due to the necessary presence of magnetization gradients induced by amorphous sinks in the large crystallites (about 100 nm thick [9]), this loss in efficiency with decreasing θ should strongly affect the long $T_{1\rho}^{\theta}$ component intensity $I_{L\rho}$ [5, 8]. $I_{L\rho}$ is found to be independent of θ (Fig. 6) and, therefore, we propose that the sinks are inside the crystallites. Suppose that the sinks are a few small mobile parts of the chains associated with conformational « defects », the large remaining crystalline phase being under rigid-lattice conditions. This situation is similar to rotating methyl groups in n-alkanes [17]. To the first approximation, the resulting $(T_{1\rho}^{\theta})_L$ can be considered as the sum of the durations of the two following steps :

(i) spin diffusion towards a sink in a time $T'_{1\rho} = R^{-1}$;

(ii) relaxation in the sink in a time $T''_{1\rho}$ given by equation (2). The deduced variation of $(T_{1\rho}^{\theta})_L$ is effectively in good agreement with both the experimental $(T_{1\rho}^{\theta})_L$ and $I_{L\rho}$ data (Figs. 5a and 6). From the minimum in $(T_{1\rho}^{\theta})_L$ (Fig. 4) one sees that the correlation time in the sink should be about 2 μs around − 10 °C.

The minimum of the short component $(T_{1\rho}^{\theta})_S$ has to be attributed to the amorphous β relaxation or « glass transition » [18-20]. However, it can be seen that $(T_{1\rho}^{\theta})_S$ is longer than predicted by the T_1 and TOE results (Tab. I, Sect. 4.2.3). An explanation is provided by the

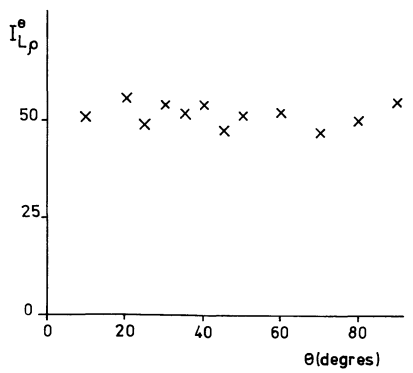

Fig. 6. — Long component intensities of the $T_{1\rho}^{\theta}$ data of figure 5.

influence of the low frequency γ-process which has been attributed to restrained chain motion in the amorphous regions [9].

4.2 RELAXATION IN THE LABORATORY FRAME. — There are now two ways of explaining the two-exponential ^1H and ^{19}F spin relaxation :

(i) a homogeneous system containing two spin species in strong dipolar interaction generally gives a two-exponential decays [6] ;

(ii) it is well established that non-exponential relaxation can arise from the presence of discrete regions of different mobilities [21]. Furthermore, these regions may interact by spin diffusion [5, 8].

In our system consisting of at least two phases, the combination of (i) and (ii) would lead to four-exponential decays. It is however not easy to detect such decays and our experimental signals have quite nicely been fit to two-exponential curves. We shall at first examine T_1 (^1H, ^{19}F) and the cross-relaxation data separately to show the difficulties encountered.

4.2.1 *T_1 Relaxation data.* — A two-exponential analysis of the experimental results is of course possible if one of the two phenomena (i) or (ii) has a negligible effect on the relaxation. Considering the T_1 relaxation only, all the conclusions are for effect (ii) :

— two-exponential signal due to the cross-relaxation effects would imply the same relaxation components in the IR of both nuclei and in the TOE [14] ;

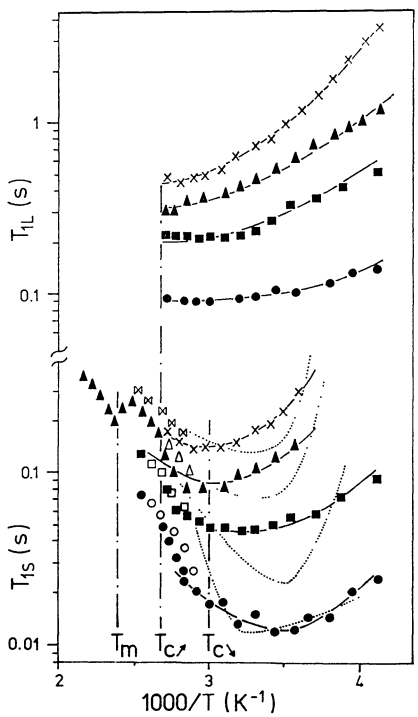

Fig. 7. — T_1 data as a function of temperature at different frequencies. ^1H resonance : ν_L = 8 (○, ●), 21 (□, ■) and 60 MHz (△, ▲) ; ^{19}F resonance : 56.4 MHz (×, ⋈). Filled symbols, heating ; open symbols, cooling from the paraelectric phase. The calculated values according to table I are shown as full curves using the HP amorphous correlation function. The dotted curves represent the calculations with the BPP correlation function when deviating from the full curves.

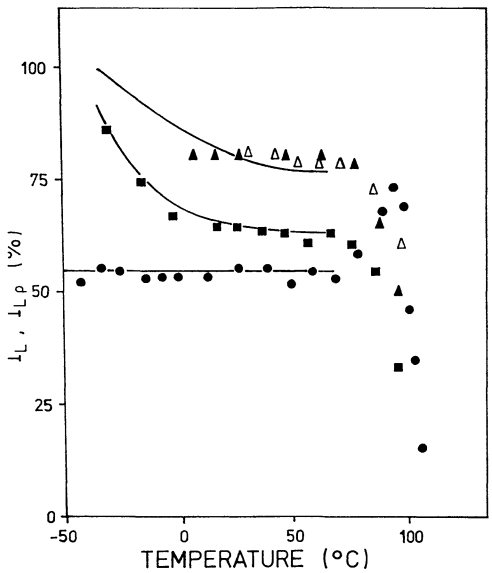

Fig. 8. — Long component intensities as a function of temperature in the heating run. I_L from T_1 in ^1H resonance at $\nu_L = 21$ MHz (■), 60 MHz (▲) and in ^{19}F resonance at $\nu_L = 56.4$ MHz (△). $I_{L\rho}$ from $T_{1\rho}$ in ^1H resonance (Fig. 4) (●). The curves have the same meaning as in figure 7.

— the intensities of the long and short components are equal in ^1H and ^{19}F resonances ;

— the T_1 relaxation is still two-exponential above 70 °C whereas there is no longer a cross-relaxation effect ;

— when analysing the FID signals corresponding to different recovery times after the inversion of the magnetization, it has been observed that the tail of the FID (corresponding to the amorphous part) is relaxing faster than the begining part (corresponding to the crystal).

4.2.2 *Cross-relaxation data.* — McBrierty and Douglass [13, 14] have shown that Solomon's equations should adequately represent spin relaxation in partly fluorinated polymers. Indeed, the T_{1+}, T_{1-} and I_+ values given by the two-exponential fittings allow us to calculate the relaxation rates ρ, ρ', σ and σ' of the Solomon's equation [14]

$$\begin{aligned} \frac{dI}{dt} &= \rho I - \sigma' S \\ \frac{dS}{dt} &= -\sigma I - \rho' S \end{aligned} \tag{4}$$

where $I = I_z - I_0$ and $S = S_z - S_0$ are, respectively, ^1H and ^{19}F magnetization along the applied field H_0 ; I_0 and S_0, the equilibrium values of ^1H and ^{19}F magnetization. The relaxation rates are written [4, 15]

$$\rho = 2/3\ \Delta M_2^{HH}\{J(\omega) + (4J(2\omega))\} + \alpha \tag{5}$$

$$\rho' = 2/3\ \Delta M_2^{FF}\{J(0.94\omega) + 4J(1.88\omega)\} + \alpha N_H/N_F \tag{6}$$

$$\sigma' = 1/2\ \Delta M_2^{HF}\{-J(0.06\omega) + 6J(1.94\omega)\} \tag{7}$$

$$\sigma = \sigma' N_H/N_F \tag{8}$$

with

$$\alpha = 1/2\ \Delta M_2^{HF}\{J(0.6\ \omega) + 3\,J(\omega) + 6\,J(1.94\ \omega)\} \tag{9}$$

where N_H and N_F are, respectively, the number of ^1H and ^{19}F spins.

The resulting maximum in $-\sigma'$ at 28 °C (Fig. 11b) has to come from the dominance of the mutual spin flip term $J(0.06\ \omega)$ in equation (7). The location of the minimum on the transition map built from the dielectric results (Fig. 12) reveals that, as in the homopolymer PVF_2 [13], this relaxation is due to the « glass transition » in the amorphous phase [18-20]. The fact that the large decrease of $-\sigma'$ begins at T_g is a clear confirmation of this. $(\rho)^{-1}$ and $(\rho')^{-1}$ (Fig. 11a) which are controlled by spectral density terms around ω (Eqs. (5) and (6)) show the same behavior as T_{1+} and T_{1-} (Fig. 9). However, it is easily checked from equations (4, 9) and the T_1 relaxation results that ρ, ρ' and $\sigma(\sigma')$ cannot be directly related to the dynamics in the amorphous phase. It is therefore concluded that a quantitative evaluation of the spin diffusion rate must be introduced in the description of the spin-lattice relaxation. This will be the aim of the next section.

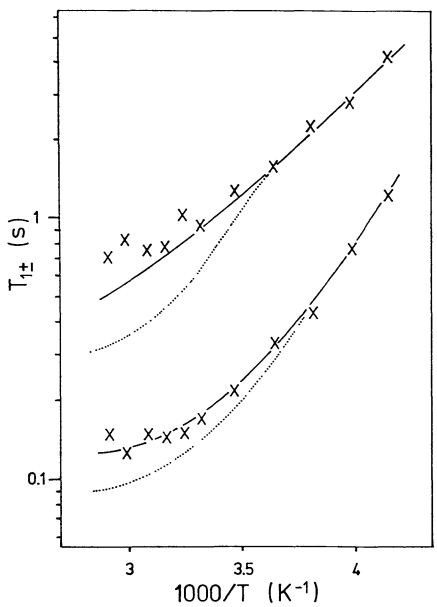

Fig. 9. — $T_{1\pm}$ data as a function of temperature. The curves have the same meaning as in figure 7.

4.2.3 *A model conciliating the relaxation and cross-relaxation results.* — To account for the effect of spin diffusion on the relaxation we use the simple model proposed by Douglass and McBrierty [5] consisting of a two-phase system where an average spin temperature is assigned to each phase. The approximation of uniform spin temperature throughout each phase may appear « unphysical » when one knows that the spin diffusion efficiency at the boundary is probably comparable to that within each phase. However, the following remarks show that this approximation should not be too bad :

— according to the $T_{1\rho}^{\theta}$ results (Sect. 4.1), the relaxation at the crystalline sinks has to be slower than spin diffusion between the sinks on the T_1 time scale ($T_1 = T_{1\rho}^{\theta}$ when

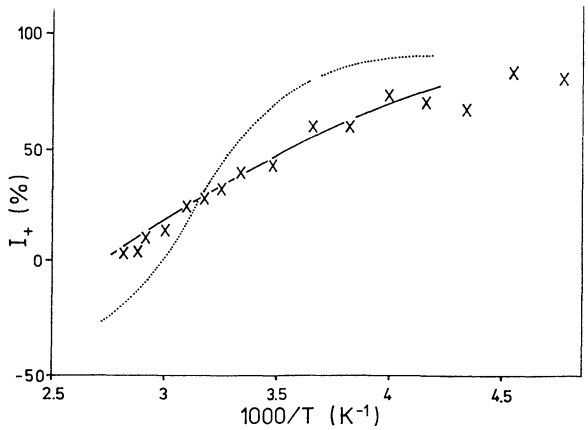

Fig. 10. — I_+ data as a function of temperature. The curves have the same meaning as in figure 7.

$\theta = 0°$). These sinks then should not create any significant spatial dependence of the magnetization within the crystalline phase ;

— due to the relatively weak difference between the two T_1 relaxation components, the amorphous phase cannot be considered as a sink, at least at 60 MHz (Fig. 7) ;

— computer simulations [8] have confirmed that the basic effects of spin diffusion on the relaxation are consistent with those predicted by chemical exchange processes between two resonance lines [22] (the attribution of an average spin temperature to each phase results in treating spin diffusion similarly to a simple exchange process [5]).

The strength of the spin diffusion coupling is then completely described by the parameters K_a and K_c related to each other by $\chi K_c = (1 - \chi) K_a = K'$ where χ is the crystalline fraction. The spin diffusion coupling takes therefore the same forms as Solomon's equation (4) so that, neglecting heteronuclear spin diffusion [4], the crystalline (c-subscript) and amorphous (a-subscript) magnetizations are controlled by the first order differential equations :

$$\begin{aligned}
\frac{dI_c}{dt} &= -(\rho_c + K_c) I_c - \sigma'_c S_c + K_a I_a \\
\frac{dS_c}{dt} &= -\sigma_c I_c - (\sigma'_c + K_c) S_s + K_a S_a \\
\frac{dI_a}{dt} &= K_c I_c - (\rho_a + K_a) I_a - \sigma'_a S_a \\
\frac{dS_a}{dt} &= K_c S_c - \sigma_a I_a - (\rho'_a + K_a) S_a .
\end{aligned} \tag{10}$$

For simplicity, the spin diffusion coupling have been taken equal within each spin species set. The numerical resolution of this system leads to a sum of four exponential decays

$$I \text{ (or } S) = I_0 \text{ (or } S_0) \sum_{n=1}^{4} I_n \exp(-R_n t) . \tag{11}$$

The relaxation rates R_1 to R_4 are arbitrarily numbered according to increasing values. According to the $T_{1\rho}^{\theta}$ results, it appears first of all reasonable to neglect the cross-relaxation within the « rigid lattice » crystalline phase [4] where the relaxation occurs *via* homonuclear

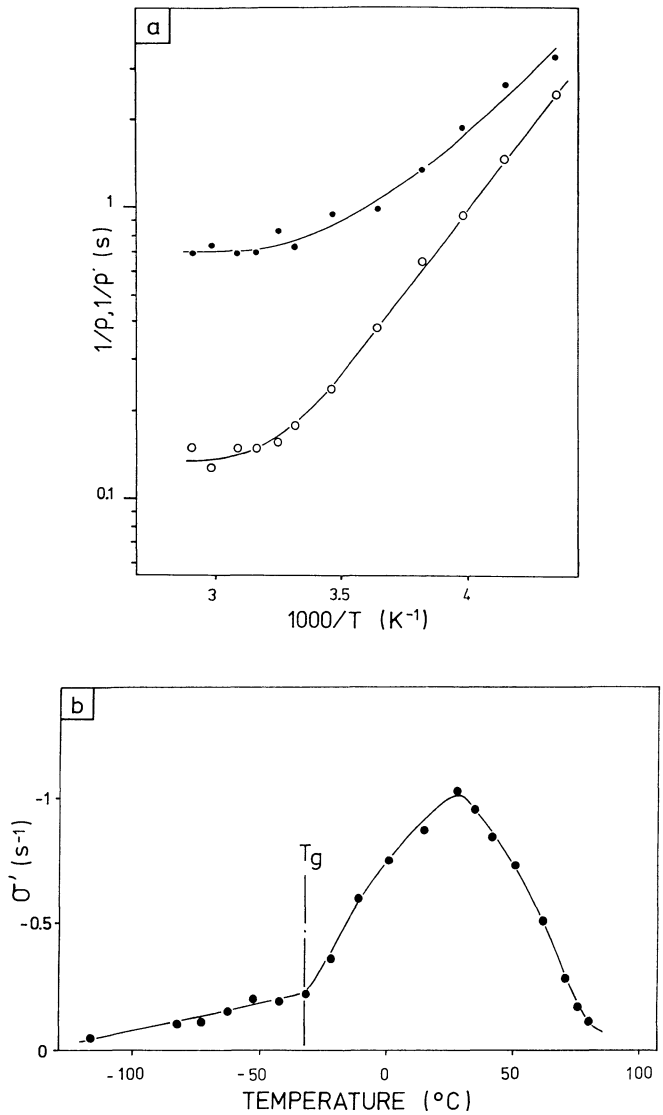

Fig. 11. — Temperature variation of the two ρ's (a) and σ's (b) determined from the cross-relaxation data. T_g is the « glass transition » temperature [20].

spin diffusion towards crystalline sinks ($\sigma_c = \sigma'_c = 0$). Since the locations of maxima are much less dependent on the correlation function the variation of the correlation time of the amorphous motion is taken from the maximum in $-\sigma'$ determined in the preceding section combined with the action energy deduced from dielectric measurements [18] (67 kJ/mol) (Fig. 12). For reasons described later we have actually used two different correlation functions : the Bloembergen Purcell Pound (BPP) [23] correlation functions associated with an isotropic reorientation $\varphi(\tau) = \exp(-\tau/\tau_c)$ and the Hunt and Powles (HP) [24] correlation functions associated with a one-dimensional diffusion process

$$\varphi(\tau) = \exp(\tau/\tau_c) \,.\, \text{erfc}\,((\tau/\tau_c)^{1/2}) \,.$$

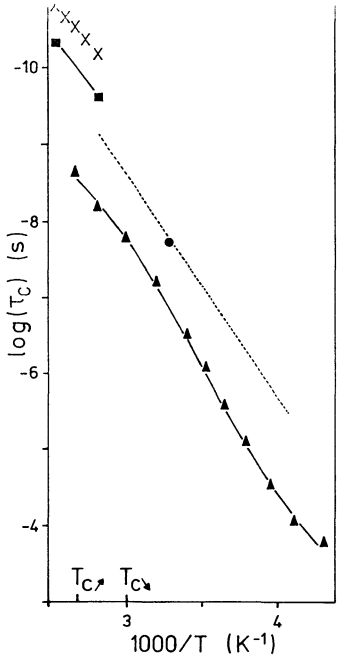

Fig. 12. — Correlation times as a function of temperature : deduced from dielectric relaxation measurements of Furukawa *et al.* [18] (▲) ; in the paraelectric phase (Part. II), from T_1 (×) and $T_{1\rho}$ (■) measurements ; the broken curve represents the variation of the NMR correlation time of the amorphous motion taken from the maximum in $-\sigma'$ (●) with an activation energy of 67 kJ/mole.

The uncritical relative magnitude of the homo and heteronuclear ΔM_2 fractions are taken from the calculation for rod-like rotation and translation of the chains $\Delta M_2^{HH} \simeq 1.8\, \Delta M_2^{FF} \simeq 4.5\, \Delta M_2^{HF}$ (see Part II). The variations of the amorphous relaxation rates ρ_a, ρ_a', σ_a and σ_a' are then given by equations (5 to 9). All the other parameters (Tab. I) are adjusted by trial and error to provide the best agreement with the experimental data, as will be seen below. The presence of limiting cases and the specific effect of each parameter on the resulting decays allow good confidence in the adjustments to fit the experimental data.

Generally, when the relaxation rates become comparable with K' the intensity is transferred, as expected [5], to the slowest relaxation rates R_1 and R_2 both in the IR and TOE experiments i.e. I_3 and I_4 become negligible. Therefore, at low temperatures ($T < 0$ °C), IR and TOE decays tend to be, respectively, one and two-exponential in agreement with the experimental data (Figs. 7 and 13). Since the crystalline and amorphous phases are then highly coupled R_1 and R_2 depend both on the crystalline and amorphous relaxation rates. A distinction between the BPP and HP correlation functions is then expected to be difficult. The important feature is that the considerable TOE can be introduced by a moderate coupling constant K' and that I_+ is then mainly a function of the magnitude of the cross-relaxation effect in the amorphous phase. With increasing temperature and amorphous relaxation rates, the spin diffusion coupling between the crystalline and amorphous phases becomes much weaker so that $(I_3 + I_4)/2$ progressively tends towards the amorphous fraction and the slow (R_1, R_2) and fast (R_3, R_4) eigenvalues are mainly controlled by, respectively, the crystalline and amorphous relaxation rates. Due to the absence of cross-relaxation in the crystalline

Table I. — *Adjusted parameters according to equation* (5-8, 10) *and figures* 7-10 *and* 12. *Error level is estimated at* 10 % *by trial and error.*

Parameters		HP c.f.	BPP c.f.
$\Delta M_2^{HH}(G^2)$		7.0	4.2
K' (s^{-1})		0.5	
χ (%)		50-60	
ρ_c (s^{-1}) from − 35 °C to 60 °C	60 MHz	from 0.7 to 1.8	
	21 MHz	from 2 to 4	
	8 MHz	from 5 to 10	
ρ_c' goes from $\rho_c/3$ to $\rho_c/2$; $\sigma_c = \sigma_c' = 0$			

Table II. — *Calculated parameters of equation* (11) *at* 60 MHz *according to table* I *(HP correlation function) ;* ρ_c *and* ρ_c' *are respectively equal to* 0.8 *and* 0.26 s^{-1} *at* − 35 °C *and* 1.6 *and* 0.7 s^{-1} *at* 27 °C.

Parameters		− 35 °C	27 °C
R_n, n = 1 to 4 (s^{-1})		0.26, 0.75, 3.2, 3.7	1.2, 2.1, 3.8, 8.4
I_n = 1 to 4	^{1}H IR (a) and (d)	−0.21, −1.78, −0.01, <1 %	−0.05, −1.44, −0.01, −0.40
	^{19}F IR (b) and (e)	−1.78, −0.22, <1 %, <1 %	−1.65, <1 %, −0.17, −0.18
	TOE (c) and (f)	−0.66, 0.66, <1 %, <1 %	−0.38, 0.15, −0.03, 0.26

Table III. — *Computed lattice sums of equation* (12) *for the all-trans* β *form according to references* [9] *and* [11].

Lattice sums (G^2)	Intra	Inter	Total
S_0	12.0	2.2	14.2
S_2	− 2.4	− 0.6	− 3.0
S_4	12.4	−0.5	11.9

Table IV. — *Deduced* NMR *orientation parameters according to equation* (12), *figure* 16 *and table* III. *The comparison with the X-ray data gives* $\chi = 0.5 \pm 0.1$. *Given the experimental accuracy of moments* (0.5 G^2), *the orientation parameters are determined at* 10 %.

NMR		X-ray[9]	
$\overline{\chi P_2(\Delta)}$	0.38	$\overline{P_2(\Delta)}$	0.70
$\overline{\chi P_4(\Delta)}$	0.14	$\overline{P_4(\Delta)}$	0.36
P_4/P_2	0.4	P_4/P_2	0.5
NMR + X-ray			
χ from P_4 data		0.54	
χ from P_2 data		0.39	

phase, I_2 (I_1) is negligible and R_1 (R_2) which is found close to $\rho_c' + K'$ ($\rho_c + K'$) can be assimilated to the slow component $(T_{1L})^{-1}$ in ^{19}F (^1H) resonance. The short component T_{1S} is then adequately attributed to the weighted sum $(I_3 + I_4)/(I_3 R_3 + I_4 R_4)$, and a comparison between the two-exponential fittings of the experimental decays and the four-exponential calculations is therefore possible (Figs. 7, 8 and 13). The computed I_L appears to mostly depend on the magnitudes of the relaxation rates relative to K' and does not allow one to significantly distinguish between the HP and BPP amorphous correlation functions and, even, between ^1H and ^{19}F resonance (60 and 56.4 MHz). The introduction of different ^1H and ^{19}F spin diffusion couplings would in any case remove the remaining difference. It is noted that the measurements of T_1 at 8 MHz are particularly useful in determining the ΔM_2 values since K' is then always much smaller than all the relaxation rates. As expected, the calculated short component T_{1S} which is very slightly sensitive to the spin diffusion clearly shows that the BPP correlation function cannot provide good agreement with the experiment. In the TOE decays, the sums of the component intensities having the same sign are always found equal to each other i.e. when $\sigma_a < 0 (> 0)$ I_1, $I_3 < 0 (> 0)$ and I_2, $I_4 < 0 (> 0)$ with $I_1 + I_3 = -(I_2 + I_4)$. $(T_{1-})^{-1}$ and $(T_{1+})^{-1}$ may, respectively, correspond to the weighted sum of R_1, R_3 and R_2, R_4 while the Overhauser effect amplitude I_+ is adequately described by $I_2 + I_4$ (Fig. 13). A comparison with the experimental results is then also possible at high temperatures (Figs. 3 and 10). Unlike I_L, we have checked numerically that, as already mentioned, I_+ is very dependent on the strength of the TOE within the amorphous phase. The origin of this general property can be traced as follows : while the direct energy transfer to the lattice is influenced by the strength of the coupling between the two phases the exchange between the two spin species in the absence of crystalline cross-relaxation requires an efficient cross-relaxation in the amorphous phase (Fig. 14). At low temperatures, it has also been observed that I_+ decreases with increasing $|\rho_c - \rho_c'|$. However, this effect appears to be unimportant since we have checked that the necessary large variation of $|\rho_c - \rho_c'|$ would be incompatible with the $T_{1\pm}$ and T_{1L} experimental values. Figure 10 shows that the computed I_+ effectively decreases more rapidly and becomes negative using the BPP correlation function, as it must be (see Part II, Fig. 5). The decrease in the spin diffusion

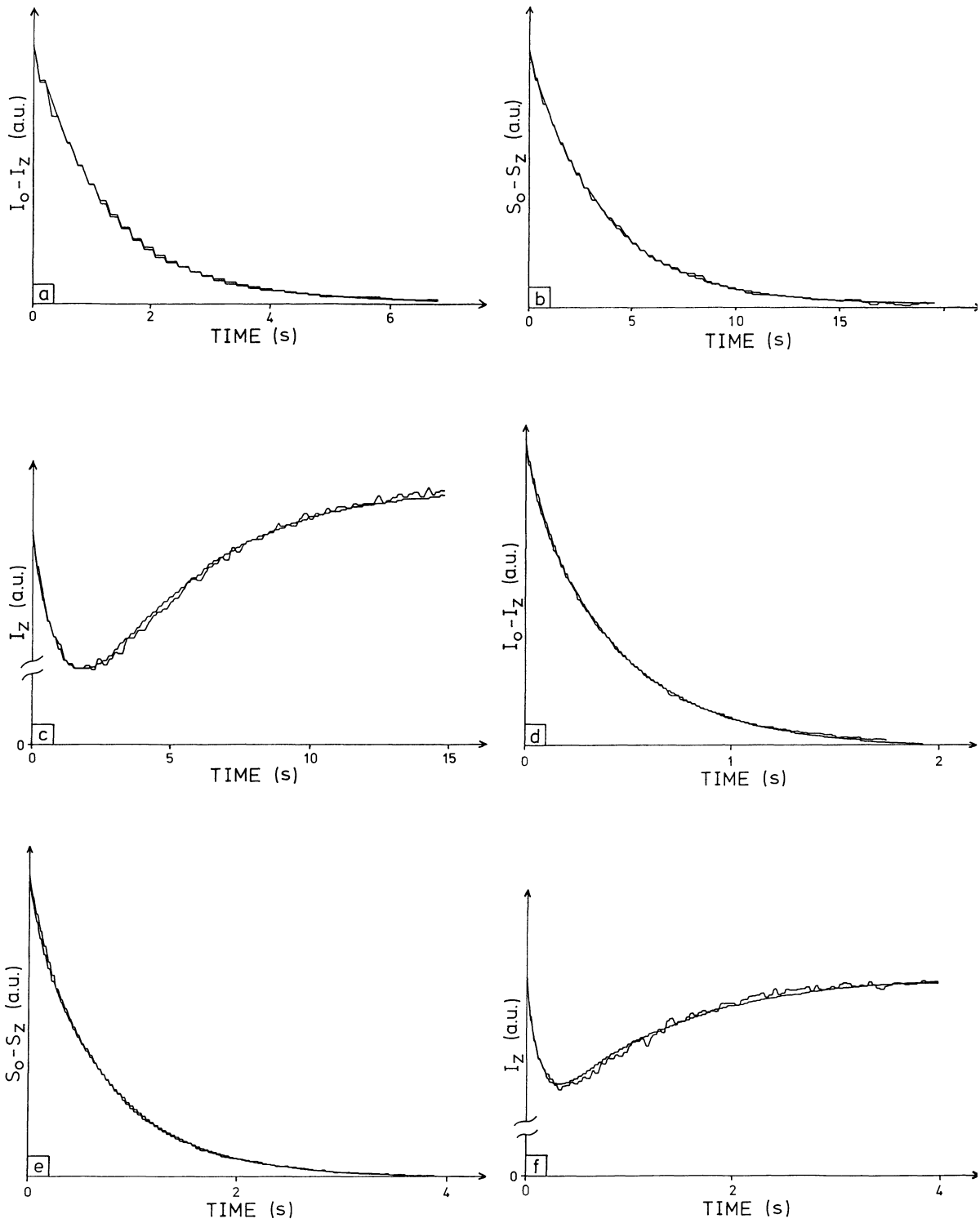

Fig. 13. — Comparison between the experimental and calculated decays of table II by the IR (^{1}H and ^{19}F resonance) and TOE sequences at − 35 °C (a, b and c) and at 27 °C (d, e and f).

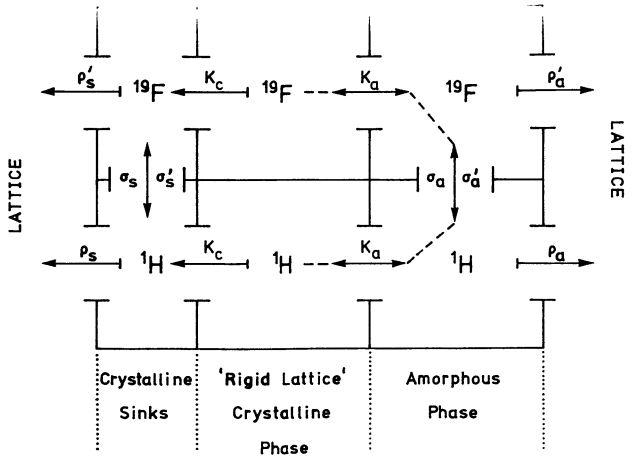

Fig. 14. — A schematic representation of the magnetization reservoirs and their possible couplings between themselves and towards the lattice. The broken line indicates the only possible pathway for cross-relaxation in the crystalline phase.

coupling with increasing temperature which progressively makes impossible the cross-relaxation *via* the amorphous phase is basically a consequence of the increase of the amorphous relaxation rates and thus reflects the nature of the amorphous correlation function. The crystalline relaxation has a noticeable effect on the $T_{1\pm}$ values only at low temperature so that an agreement with the experiment is possible below 0 °C for the BPP correlation function (Fig. 9). Although the description of our system involves too many parameters to obtain crystalline relaxation rates, especially at low temperature, ρ_c and ρ_c' undoubtedly have to increase with increasing temperature implying that τ_c in the crystalline sinks is higher than 10^{-8} s (Tab. I).

In conclusion, unlike the nonexponential HP correlation function, the BPP c.f. is not able to describe the molecular motion in the amorphous phase. This, of course, is no proof that the HP correlation function is the only one possible. This choice is motivated by the study of the paraelectric phase (Part II) in order to explain the continuous dynamical behavior through the Curie transition which has been demonstrated by dielectric relaxation studies [18, 19]. The adjusted crystalline fraction (50-60 %) is confirmed by the M_2 measurements on the oriented sample (Appendix) and is in agreement with X-ray [25] and D-E hysteresis [26] studies performed on samples which undewent similar thermal treatments. χ is nevertheless found to be less than the « rigid » content deduced from previous line-shape studies with an exponential fitting of the tail of the FID [11, 27] (80 to 90 %). In agreement with spin relaxation in the paraelectric phase (Part II), we propose that this discrepancy is due to a nonexponential amorphous decay resulting from the anisotropy of the motion. When assuming the low temperature FID for the crystalline phase which is relaxed by localized sinks, figure 15 demonstrates the Gaussian form of the amorphous signal. Moreover, the decrease in the second moment fits well with the ΔM_2 values of table I. The deduced coupling constant K' demonstrates the slowness of the spin diffusion between the crystalline and amorphous phases. Such a result agrees with the fact that the amorphous regions are not likely to constitute efficient relaxation sinks.

Moreover, considering the domain sizes (ca 100 nm) [9], it would imply that the spin diffusion coefficient is smaller than in fully hydrogenated [8] or fluorinated systems [5].

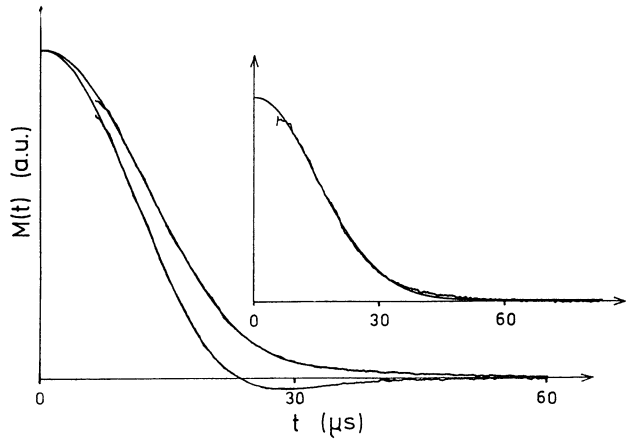

Fig. 15. — ^{1}H FID at − 130 °C ($M_2 = 13.5 \pm 0.5$ G^2) and 27 °C ($M_2 = 9.8 \pm 0.5$ G^2). The difference between the room temperature FID and the weighted (crystallinity 55 %) low temperature FID is fitted in the insert with a Gaussian of $M_2 = 6.1 \pm 0.05$ G^2.

4.3 IN THE TRANSITION RANGE (FROM 60 TO 110 °C). — Figures 4, 7 and 8 reveal that the long relaxation component associated with the ferroelectric phase vanishes above T_c in both laboratory and rotating frames, as it must. The absence of a discontinuity in T_{1S} through the first-order ferroelectric transition implies a great similarity between the high frequency motions in the paraelectric phase and in the amorphous part below T_c. Such an asssumption will be confirmed in part II. On the other hand, the clear discontinuity in T_{1S}^{ρ} would be in agreement with the disappearance of the low frequency γ-process [19].

However, figure 8 shows a rather puzzling behavior of $I_{L\rho}$: while the transformation from a ferroelectric to paraelectric phase is almost perfectly reflected by I_L, $I_{L\rho}$ increases when the transition is approached.

It must nevertheless be noted that, just above T_c on heating (100 °C), since $I_{L\rho}$ agrees well with the fraction of ferroelectric phase [11] (Fig. 8) the ferroelectric and paraelectric phases

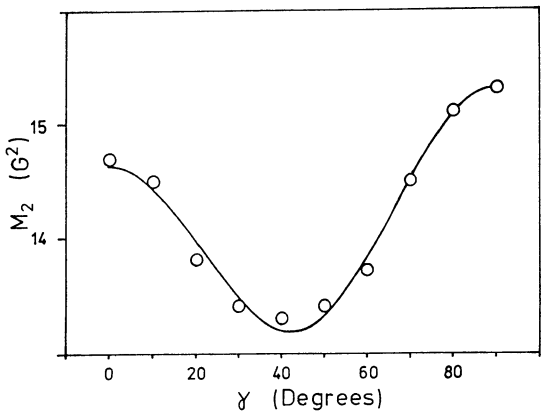

Fig. 16. — Anisotropy of M_2 in rigid lattice conditions ($T = -130$ °C) for the oriented sample with a best fit according to equation (12), $C_0 = 14.14 \pm 0.02$, $C_2 = -1.13 \pm 0.02$ and $C_4 = 1.62 \pm 0.02$.

can again be regarded as non-interacting. We then conclude that this « anomalous $I_{L\rho}$ behavior » is intimately related to the considerable morphological changes taking place during the ferroelectric transition [9].

Conclusion.

The simultaneous study of ^1H and ^{19}F relaxation in the laboratory frame and at different angles to H_0 in the rotating frame, together with the transient Overhauser experiment and the FID analysis give, except in the transition range where some doubts remain, a consistent picture of the coupling to the lattice in the ferroelectric phase. In particular, when compared with the results in the paraelectric phase (Part II), the shape of the correlation function in the amorphous phase confirms the strong experimental hints for a similar high frequency mode both below and above T_c [18, 19] (Fig. 12). Another finding is the existence of efficient « sinks » in the crystalline phase. These should be related to the presence of conformational defects which probably have an important role in the initiation of the Curie transition. Measurements on poled samples or with a different TrFE content may be useful in relating the defect concentration to the ferroelectric domains or the chemical microstructure of the chains. It should however be pointed out that similar defects could exist in pure PVF_2 as a consequence of the fraction of head-to-head or tail-to-tail addition [28].

Appendix.

LINE SHAPE ANISOTROPY ANALYSIS FOR THE ORIENTED SAMPLE. — Assuming a uniaxial orientation of the crystallites embedded in an isotropic amorphous rigid matrix the anisotropy of the total second moment is given by [29, 30]

$$M_2(\gamma) = C_0 + C_2 P_2(\cos\gamma) + C_4 P_4(\cos\gamma)$$

with

$$C_0 = \chi S_0 + (1-\chi) M_{2a} \qquad (12)$$

$$C_2 = \chi S_2 \overline{P_2(\cos\Delta)}$$

$$C_4 = \chi S_4 \overline{P_4(\cos\Delta)}$$

where P_2 and P_4 are Legendre polynomials. γ and Δ are the angle between the drawing direction and, respectively, the applied field H_0 and a crystallite axis, the bar denoting the average over the sample. χ is the crystallite fraction and M_{2a} is the rigid-lattice amorphous second moment. S_0, S_2 and S_4 are lattice sums which depend on the polymer structure and dynamics [31]. X-ray [9, 20, 32] and infrared [20] studies clearly demonstrate that the 70/30 VF_2/TrFE copolymer directly crystallizes in the extended all-trans conformation (β-form). We have then computed S_0, S_2 and S_4 for this crystalline conformation with the same assumptions as in reference [11] and the lattice parameters measured on a similar sample [9] (Tab. III).

The « rigid-lattice » ^1H total second moment has been measured by the POLFIT procedure [12] at -130 °C. Figure 16 shows the variation of M_2 as a function of γ. The comparison between the orientation parameters deduced from NMR and the X-ray data gives a crystalline fraction of about 50 % (Tab. IV). C_0 is found to be almost equal to S_0 : this indicates the closeness of M_{2a} and the crystalline powder average S_0 (Eq. (12)) which is consistent with the invariance of the low temperature second moment of unoriented samples upon annealing [11].

References

[1] LOVINGER A. J., Developments in crystalline polymers, Applied Science Publishers, Ed. D. C. Bassett, London (1981) I p. 195.
[2] YAMADA T. and KITAYAMA T., *J. Appl. Phys.* **52** (1981) 6859.
[3] HIRSCHINGER J., MEURER B. and WEILL G., Part. II, submitted.
[4] ABRAGAM A., The principles of nuclear magnetism (Oxford, University Press, New York) 1961.
[5] DOUGLASS D. C. and MCBRIERTY V. J., *J. Chem. Phys.* **54** (1971) 4085.
[6] SOLOMON I., *Phys. Rev.* **99** (1955) 559.
[7] TSE D. and HARTMANN S. R., *Phys. Rev. Lett.* **21** (1968) 511.
[8] PACKER K. J., POPE J. M., YEUNG R. R. and CUDBY M. E. A., *J. Pol. Sci. Phys.* **22** (1984) 589.
[9] DELZENNE P., Ph. D. Thesis, University of Grenoble (1986).
[10] STOKES H. T. and AILION D. C., *Phys. Rev. B* **18** (1978) 141.
[11] HIRSCHINGER J., MEURER B. and WEILL G., *Polymer* **28** (1987) 721.
[12] MEURER B., SPEGT P. and WEILL G., *J. Phys. E: Sci. Instrum.* **16** (1983) 403.
[13] MCBRIERTY V. J. and DOUGLASS D. C., *Macromolecules* **10** (1977) 855.
[14] DOUGLASS D. C. and MCBRIERTY V. J., *Macromolecules* **11** (1978) 766.
[15] O'REILLY D. E., PETERSON E. M. and TUNG TSANG, *Phys. Rev.* **160** (1967) 333.
[16] LEE M. and GOLDBURG W. I., *Phys. Rev.* **140** (1965) A 1261.
[17] DOUGLASS D. C. and JONES G. P., *J. Chem. Phys.* **45** (1966) 956.
[18] FURUKAWA T., OHUCHI M., CHIBA A. and DATE M., *Macromolecules* **17** (1984) 1384.
[19] KOIZUMI N., HAIKAWA N. and HABUKA H., *Ferroelectrics* **59** (1984) 99.
[20] YAGI T., TATEMOTO M. and SAKO J. I., *Polymer J.* **12** (1980) 209.
[21] MCBRIERTY V. J. and DOUGLASS D. C., *Phys. Rev.* **63** (1980) 61.
[22] WOESSNER D. E., *J. Chem. Phys.* **35** (1961) 41.
[23] BLOEMBERGEN N., PURCELL E. M. and POUND R. V., *Phys. Rev.* **73** (1948) 679.
[24] HUNT B. I. and POWLES J. G., *Proc. Phys. Soc.* **88** (1966) 513.
[25] NISHI E., OBA H., MATSUDA K. and WADA Y., *Rep. Prog. Pol. Phys. Jap.* **27** (1984) 163.
[26] TAKEDA H., KOYAMA K., IKEDA S. and WADA Y., *Rep. Prog. Pol. Phys. Jap.* **28** (1985) 371.
[27] LEGRAND J. F., SCHUELE P. J., SCHMIDT V. H. and MINIER M., *Polymer* **26** (1985) 1683.
[28] LOVINGER A. J., DAVIS D. D., CAIS R. E. and KOMETANI J. M., *Polymer* **28** (1987) 617.
[29] MCBRIERTY V. J. and WARD I. M., *J. Phys. D* **2** (1968) 1529.
[30] MCBRIERTY V. J. and DOUGLASS D. C., *J. Magn. Res.* **2** (1970) 352.
[31] MCBRIERTY V. J., MCCALL D. W., DOUGLASS D. C. and FALCONE D. R., *J. Chem. Phys.* **52** (1970) 512.
[32] LOVINGER A. J., FURUKAWA T., DAVIS G. T. and BROADHURST M. G., *Polymer* **24** pp. 1223-1225 (1983).